# Improvement of Solid-State Excimer Emission of the Aryl−Ethynyl−*o*-Carborane Skeleton by Acridine Introduction

Junki Ochi, Kazuo Tanaka*, Yoshiki Chujo

*Department of Polymer Chemistry, Graduate School of Engineering, Kyoto University*

*Katsura, Nishikyo-ku, Kyoto 615-8510, Japan*

Tel: +81-75-383-2604

Fax: +81-75-383-2605

E-mail: tanaka@poly.synchem.kyoto-u.ac.jp

Key words: Carborane; solid-state luminescence; excimer

**ABSTRACT**

We report highly-efficient and solid-state excimer emission based on the acridine−*o*-carborane dyad possessing the ethynyl spacer. The previous pyrene-modified *o*-carborane showed excimer emission only at 77 K in the crystalline state, meanwhile the current acridine-modified molecule presented excimer emission with high efficiency ($\Phi_{PL}$ = 0.23) in crystalline state at room temperature. From single crystal X-ray crystallography, it was indicated that two acridine moieties were stacked and the third acridine molecule was out of alignment. Such a packing mode could restrict exciton splitting over the columnar packing structure. Moreover, molecular interactions through the nitrogen atom in the acridine moiety and the hydrogen atom in the *o*-carborane unit contributes to suppression of molecular motions. As a consequence, improvement of emission efficiency was obtained. This study demonstrates that the ethynyl−*o*-carborane skeleton should work as the excimer-inducible component in the solid state.

## INTRODUCTION

*o*-Carborane is the icosahedral cluster composed of ten boron and two carbon atoms. When aromatic moieties are connected at the carbon in the *o*-carborane unit, intense emission can be observed from the intramolecular charge transfer (ICT) state by using *o*-carborane as an electron acceptor.[1–4] It should be emphasized that ICT emission can be preserved even in the solid state where conventional organic luminescent dyes commonly provide poor luminescence due to concentration quenching.[5–25] Because of the steric structure of the *o*-carborane unit, non-specific intermolecular interaction can be efficiently disturbed even in the condensed state, followed by highly-efficient solid-state luminescent properties. On the basis of these results, we regard *o*-carborane as a conjugated "element-block",[26–27] which is the minimum functional unit consist of heteroatoms, and designed various aryl-modified molecules to obtain optical materials.[28–32] So far, the series of unique luminescent materials have been prepared by the combination of various aromatic rings, such as aggregation-induced emission,[33,34] intense solid-state luminescence with almost quantitative efficiencies in the visible region,[35,36] a highly-stable near-infrared luminophore[37] and stimuli-responsive luminochromic behaviors.[38–41] Except for these materials, wide variety of solid-state luminescent *o*-carboranes have been recently discovered. Thus, it can be said that *o*-carborane should be a versatile platform for designing advanced optoelectronic materials.[42,43]

More recently, it was shown that solid-state luminescence attributable to the excimer formation was induced by inserting the ethynyl spacer between *o*-carborane and the aromatic moiety.[44] By cooling the crystalline sample at 77 K, drastic luminescent

chromism between orange emission from the ICT state and green one from the excimer was able to be observed. This means that thermochromic luminescence was accomplished by cooling with the pyrene−ethynyl−*o*-carborane structure. These data also implied that the ethynyl−*o*-carborane unit is the excimer-inducible "element-block" in the solid-state. To prove the validity of this idea, further examples to offer solid-state excimer emission should be needed with different types of aromatic rings. Additionally, emission efficiency in the solid state was critically lowered by introducing the ethynyl spacer (emission quantum yield $\Phi_{PL} < 0.01$ in solution and $\Phi_{PL} = 0.09$ in crystal). It is likely that molecular tumbling vigorously occurred at the ethynyl-linked *o*-carborane unit, followed by emission quenching. Thus, we sought a next aryl-modified *o*-carborane with the ethynyl spacer which shows excimer emission with high efficiency in the solid state.

Herein, we report excimer emission of the acridine−ethynyl−*o*-carborane molecule **CBAc** at room temperature in the crystalline state. By employing acridine at the aromatic moiety, it was presumed that luminescence from the locally-excited (LE) state of the aromatic moiety, which is the favorable electronic structure for the formation of excimer state, was able to be enhanced by suppressing the formation of the ICT state. Moreover, we also expected that molecular motions in the solid state could be restricted by interaction at the endocyclic nitrogen in the acridine moiety. In order to prove the versatility of this molecular design consist of the ethynyl−*o*-carborane unit for fabricating solid-state luminescent materials, synthesis and evaluation of optical properties have been conducted.

## RESULTS AND DISCUSSION

Scheme 1 shows the synthetic route of **CBAc**. 9-Iodoacridine was prepared from 9-bromoacridine[45] and immediately used in Sonogashira−Hagihara cross coupling reaction with 1-ethynyl-*o*-carborane.[46] The product was characterized by $^{1}H$, $^{13}C$ and $^{11}B$ NMR spectroscopies, high resolution mass spectroscopy and single crystal X-ray crystallography. From these data, we concluded that **CBAc** having the designed structure can be obtained in good yield. **CBAc** showed good solubility in common organic solvents such as chloroform ($CHCl_3$), dichloromethane and tetrahydrofuran (THF). The yellow-luminescent crystal which was applicable for the single crystal X-ray analysis was obtained through recrystallization in the $CHCl_3$/hexane mixture solvent. Structural and optical measurements in the solid state were performed with this crystalline sample.

Scheme 1

Figure 1 illustrates the result from the single crystal X-ray analysis with **CBAc** (Table S1). Two types of the dimer structures were observed, that is, the π-dimer including π-π interaction between two acridine moieties and the N-dimer including N-H interaction between the nitrogen atom of the acridine moiety and the hydrogen atom of the *o*-carborane unit. These two types of dimers are stacked alternately and formed columnar packing. According to the top views of these dimers, two aromatic rings are overlapped widely in the case of the π-dimer, while there is little overlap of the aromatic rings in the N-dimer. Thereby, in the crystalline state of **CBAc**, only two acridine molecules have strong interaction. The third acridine molecule is out of alignment by the restriction of N-H interaction.

Figure 1

To evaluate electronic structures of **CBAc**, optical measurements were performed in $CHCl_3$ (Figure 2, Table 1). The vibrational structure attributable to the π−π* transition of the acridine moiety was clearly observed in the UV−vis absorption spectrum between 350 and 450 nm.[47] This fact means that electronic interaction should be hardly formed in the ground state through the ethynyl spacer. The corresponding result was observed from the photoluminescence (PL) spectrum. The emission band from the LE state of the acridine moiety was measured from the same solution, indicating the electronic structure at the acridine moiety should be also isolated from the *o*-carborane unit in the excited state. The similar absorption spectrum was observed from the solution of the pyrene-substituted dyad with the ethynyl spacer.[44] In the solution state, the ethynyl spacer plays a role in separating electronic interaction between *o*-carborane and aromatic rings. Meanwhile, the critical change in the PL spectrum was observed from the crystalline sample (Figure 2, T a b l e 1 ) .

Figure 2 and Table 1

T h e

To elucidate the origin of the long-lifetime emission of the **CBAc** crystal, further PL measurements were conducted under various conditions. As mentioned in the introduction on the basic emission mechanism of aryl−*o*-carborane dyads, the aryl-substituted *o*-carboranes showed the ICT emission in the longer wavelength region rather than the LE emission.[47] According to these studies, it was already known that PL spectra of *o*-carborane derivatives with ICT character have two features:[48] First, intensity of the ICT emission is lowered and the position is red-shifted by increasing solvent polarity. Second, dual emission consist of the LE and ICT emission band is often observed at 77K where the molecular motions are completely frozen. Significantly, in contrast to these characters from the ICT emission, **CBAc** showed no new emission bands in the longer-wavelength region in highly-polar solvents, supporting that the emission bands should be from the LE state (Figure S1). It should be noted that only the LE emission band was observed in the frozen matrix (2-methylTHF, $1.0 \times 10^{-5}$ M at 77K, Figure S2). This fact strongly suggests that the emission band in the crystalline state should be induced not from the ICT state but from the intramolecular interaction in the crystalline packing.

To investigate the influence of intramolecular interaction and molecular motions in details, we compared luminescent properties in the polymer matrix and those in the condensed state. PL spectra were measured with the cast film of **CBAc** and the homogeneous **CBAc**-loaded film (1 wt%) with poly(methyl methacrylate) (PMMA) where **CBAc** molecules should be isolated each other (Figure 2). Apparently, the LE emission was observed from the PMMA film, whereas significant yellow emission similarly to that in the crystal state was detected from the cast film in the absence of

matrices (Figure 2). These data support that yellow emission should be induced only by intermolecular interaction in the condensed state. From the cast film of **CBAc**, similar emission properties were obtained with the crystalline sample, suggesting that **CBAc** could be applicable as an ink for fabricating printing optoelectronic devices.

To demonstrate environment-depending switching of luminescent color, we performed the aggregation experiment with the solution of **CBAc** (Figure S3). By increasing the water content of the THF solution, aggregation was formed, and correspondingly emission color turned to yellow. Compared to the absorption spectra between the aggregation and crystalline states, the structural peaks were obtained at the similar positions (Figure S4). From these spectroscopic data, it was suggested that excimer emission should be obtained after aggregation formation. This result represents that the emission process can be switched from the LE state to excimer by dynamic environmental change.

To obtain deeper insight into the optical properties, quantum calculations were performed for estimating the molecular orbitals by using density functional theory (DFT) for the ground state and time dependent-DFT (TD-DFT) for the excited state. The structures of both compounds were optimized at the B3LYP/6-31+G(d,p) level in both states (Figure 3, Table S2). Accordingly, distribution of electronic orbitals was hardly observed in both states at the *o*-carborane unit. This result supports the above experimental data that the formation of the ICT state should be not capable in **CBAc**.

Figure 3

From the electrochemical measurements, the energy levels of highest occupied molecular orbital (HOMO) and lowest unoccupied molecular orbital (LUMO) were determined (Figures 4 and S5). It was clearly indicated that the energy levels were slightly influenced by the existence of the *o*-carborane unit. These data mean that electronic interaction between *o*-carborane and acridine should be hardly obtained in **CBAc**. As a consequence, not the ICT emission but the LE emission can be observed from **CBAc**.

Figure 4

Considering above data including the fact that yellow emission was detectable only in the condensed state, it can be summarized that the emission band in the longer wavelength region should be originated from the excimer of the acridine moiety in **CBAc**. Existence of π-π interaction in the π-dimer could strongly facilitate the formation of the acridine excimer according to the molecular distribution in the crystal packing.[49] In addition, π–π interaction in the N-dimer is inhibited because the relational position of two molecules are strongly locked by N-H interaction and their π-planes are spatially displaced. Such a characteristic packing mode binds exciton within each π-dimer and suppresses exciton splitting over the columnar packing structure through the N-dimer.[50] It can be also said that N-H interaction suppresses molecular vibration and rotation which induce non-radiative transition. Thus, highly-efficient and long-lifetime excimer emission can be obtained in the crystalline state.

## CONCLUSION

On the basis of the previous result that the aryl−ethynyl−*o*-carborane structure could be responsible for expressing excimer emission in the solid state, we designed and synthesized the acridine-tethered *o*-carborane with the ethynyl spacer. Despite that the pyrene-modified *o*-carborane showed excimer emission only at 77K, the resulting **CBAc** showed yellow emission with high emission quantum yield in the crystalline state even at room temperature. The result from single crystal X-ray crystallography proposed that the packing structure, degree of stacking and molecular interaction were favorable for enhancing solid-state excimer emission. This study demonstrates that the ethynyl−*o*-carborane skeleton should be the excimer-inducible "element-block" in the solid state.

## EXPERIMENTAL SECTIONS

**General.** $^{1}H$, $^{13}C$, and $^{11}B$ NMR spectra were recorded on a JEOL JNM-AL400 instrument at 400, 100, and 128 MHz, respectively. The $^{1}H$ and $^{13}C$ chemical shift values were expressed relative to $Me_4Si$ as an internal standard. The $^{11}B$ chemical shift values were expressed relative to $BF_3{\cdot}Et_2O$ as an external standard. High resolution mass (HRMS) spectrometry was performed at the Technical Support Office (Department of Synthetic Chemistry and Biological Chemistry, Graduate School of Engineering, Kyoto University), and the HRMS spectra were obtained on a Thermo Fisher Scientific EXACTIVE spectrometer for electrospray ionization (ESI) and a Thermo Fisher Scientific EXACTIVE spectrometer for atmospheric pressure chemical ionization (APCI). Analytical thin-layer chromatography (TLC) was performed with silica gel 60 Merck F254 plates. Column chromatography was performed with Wakogel C-300 silica gel. UV−vis absorption spectra were obtained on a SHIMADZU UV3600 spectrophotometer.

Photoluminescence (PL) spectra were obtained on a Horiba Fluorolog-3 luminescence spectrometer. Fluorescence quantam yield (QY) was recorded on a HAMAMATSU Quantaurus-QY Plus C13534-01 model. The PL lifetime measurement was performed on a Horiba FluoreCube spectrofluorometer system; excitation was carried out using a UV diode laser (NanoLED 375 nm). Cyclic voltammetry (CV) was carried out on a BASALS-Electrochemical-Analyzer Model 600D with a glassy carbon working electrode, a Pt counter electrode, an Ag/AgCl reference electrode, and the ferrocene/ferrocenium ($Fc/Fc^+$) external reference at a scan rate of 0.1 V $s^{-1}$. X-ray crystallographic analysis was carried out by Rigaku R-AXIS RAPID-F graphite-monochromated MoKα radiation diffractometer with imaging plate. A symmetry-related absorption correction was carried out by using the program ABSCOR.[51] The analysis was carried out with direct methods (SHELX-97[52]) using Yadokari-XG[53]. The program ORTEP3[54] was used to generate the X-ray structural diagram.

**Materials.** All synthetic procedures were performed under Ar atmosphere. Tetrahydrofurane (THF), diethyl ether and triethylamine were purchased and purified by passage through purification column under Ar pressure. *n*-BuLi in hexane, CuI, $Pd_2(dba)_3$, tri(2-furyl)phosphine (TFP) were obtained commercially and used without purification. 1-ethynyl-*o*-carborane[46] and 9-bromoacridine[50] were synthesized and characterized according to the literatures.

**9-Iodoacridine (1).** To a 100 mL round-bottomed flask containing 9-bromoacridine (0.518 g, 2.01 mmol) and anhydrous diethylether (25 mL) was added *n*-BuLi (2.8 mL, 1.6 M in hexane, 2.88 mmol) dropwise at 0 °C. After addition, the mixture was stirred for

additional 30 min at room temperature, then $I_2$ (0.844 g, 3.33 mmol) was added. This mixture was stirred for 16 h, and this solution was washed with sodium thiosulfate (aq. 25%) 5 times. The solution was then dried over $Na_2SO_4$ and evaporated *in vacuo* to afford the crude product, which was further purified by column chromatography on silica gel (hexane/THF v/v = 9/1) as a beige solid (0.325 g, 1.07 mmol, 53%). $^1$H NMR (400 MHz, $CDCl_3$): δ (ppm) 8.34 (d, *J* = 8.4 Hz, 2H), 8.19 (d, *J* = 8.8 Hz, 2H), 7.80 (m, 2H), 7.64 (m, 2H). $^{13}$C NMR spectrum was not obtained duet to poor solubility in commodity organic solvents and instability. Therefore, the product was used directly for the next step without further analyses. HRMS (ESI): calcd. for $C_{13}H_9IN$ $[M+H]^+$ m/z 305.9774, found m/z 305.9779.

**9-((1-*o*-Carboranyl)ethynyl)acridine (CBAc).** The mixture of 1-ethynyl-*o*-carborane (0.0892 g, 0.530 mmol), 9-iodoacridine (0.179 g, 0.587 mmol), CuI (0.0198 g, 0.104 mmol), $Pd_2(dba)_3$ (0.0143 g, 0.0156 mmol) and TFP (0.0184 g, 0.0793 mmol) was dissolved in 11 mL of THF and 11 mL of triethylamine under Ar atmosphere. The mixture was stirred at r.t. for 16 h, then washed with $NH_4Cl$ and brine and organic layer was dried over $Na_2SO_4$. After $Na_2SO_4$ was removed, the solvent was evaporated. The residue was purified by column chromatography on silica gel (hexane/THF v/v = 9:1). After evaporation of solvent, recrystallization from $CHCl_3$ afforded compound **CBAc** as a yellow solid (0.0443 g, 0.128 mmol, 24%). $^1$H NMR (400 MHz, $CDCl_3$): δ (ppm) 8.27 (d, *J* = 8.8 Hz, 2H), 8.22 (d, *J* = 6.0 Hz, 2H), 7.84 (t, *J* = 7.6 Hz, 2H), 7.68 (t, *J* = 7.6 Hz, 2H), 4.17 (s, 1H), 3.65-1.67 (br, 10H). $^{13}$C NMR (100 MHz, $CDCl_3$): δ (ppm) 148.4, 130.6, 130.4, 127.7, 127.0, 125.6, 123.5, 97.1, 73.7, 63.0, 60.7. $^{11}$B NMR (128 MHz, $CDCl_3$): δ (ppm) –1.2, –2.3, –7.9, –9.2, –10.5, –13.2. HRMS (APCI): calcd. for $C_{17}H_{20}B_{10}N$ $[M+H]^+$

m/z 348.2521, found m/z 348.2528. CCDC #: 1893258.

**9-((1-Trimethylsilyl)ethynyl)acridine (TMSAc).** In a 300 mL round-bottomed flask 9-bromoacridine (0.773 g, 3.00 mmol,), ethynyltrimethylsilane (0.5 mL, 0.355 g, 3.61 mmol), CuI (0.0205 g, 0.108 mmol) and $Pd(PPh_3)_2Cl_2$ (0.0408 g, 0.0581 mmol), were dissolved in THF (50 mL) and triethylamine (24 mL) under Ar atmosphere. The reaction mixture was stirred at 70 °C for 16 h and subsequently washed with $NH_4Cl$ solution and brine. The organic phase was dried over $Na_2SO_4$ and concentrated under vacuum. The residue was purified by column chromatography on silica gel (hexane/THF v/v = 20:1). After evaporation of solvent, the residue was washed by hexane to yield the product **TMSAc** as brown solid (0.303 g, 1.10 mmol, 37 %). $^1$H NMR (400 MHz, $CDCl_3$): δ (ppm) 8.47 (d, *J* = 8.4 Hz, 2H), 8.23 (d, *J* = 8.8 Hz, 2H), 7.80 (m, 2H), 7.62 (m, 2H), 0.44 (s, 9H). $^{13}$C NMR (100 MHz, $CDCl_3$): δ (ppm) 147.5, 129.3, 128.9, 126.5, 125.7, 125.7, 125.6, 110.7, 98.0, –1.0. HRMS (APCI): calcd. for $C_{18}H_{18}NSi$ $[M+H]^+$ m/z 276.1203, found m/z 276.1204.

**ACKNOWLEDGMENT**

This work was partially supported by the Asahi Glass Foundation (for K.T.) and a Grant-in-Aid for Scientific Research (B) (JP17H03067) and (A) (JP17H01220), for Scientific Research on Innovative Areas “New Polymeric Materials Based on Element-Blocks (No.2401)” (JP24102013) and for Challenging Research (Pioneering) (JP18H05356).

**References**


1. Y.-J. Cho, S.-Y. Kim, M. Cho, W.-S. Han, H.-J. Son, D. W. Cho, S. O. Kang, *Phys. Chem. Chem. Phys*. **2016**, *19*, 9702−9708.
2. S.-Y. Kim, Y.-J. Cho, G. F. Jin, W.-S. Han, H.-J. Son, D. W. Cho, S. O. Kang, *Phys. Chem. Chem. Phys*. **2015**, *17*, 15679−15682.
3. Z. Wang, P. Jiang, T. Wang, G. J. Moxey, M. P. Cifuentes, C. Zhang, M. G. Humphrey, *Phys. Chem. Chem. Phys*. **2016**, *18*, 15719−15726.
4. S. Kwon, K.-R. Wee, Y.-J. Cho, S. O. Kang, *Chem. Eur. J*. **2014**, *20*, 5953−5960.
5. R. Furue, T. Nishimoto, I. S. Park, J. Lee, T. Yasuda, *Angew. Chem. Int. Ed*. **2016**, *55*, 7171−7175.
6. S. Inagi, K. Hosoi, T. Kubo, N. Shida, T. Fuchigami, *Electrochemistry* **2013**, *81*, 368−370.
7. M. R. Son, Y.-J. Cho, S.-Y. Kim, H.-J. Son, D. W. Cho, S. O. Kang, *Phys. Chem. Chem. Phys*. **2017**, *19*, 24485−24492.
8. D. Tu, P. Leong, S. Guo, H. Yan, C. Lu, Q. Zhao, *Angew. Chem. Int. Ed*. **2017**, *56*, 11370–11374.
9. Y. Chen, J. Guo, X. Wu, D. Jia, F. Tong, *Dyes Pigments* **2018**, *148*, 180−188.
10. A. Ferrer-Ugalde, J. Cabrera-González, E. J. Juárez-Pérez, F. Teixidor, E. Pérez-Inestrosa, J. M. Montenegro, R. Sillanpää, M. Haukka, R. Núñez, *Dalton Trans*. **2017**, *46*, 2091−2104.
11. Z. Wang, T. Wang, C. Zhang, M. G. Humphrey, *Phys. Chem. Chem. Phys*. **2017**, *19*, 12928−12935.
12. X. Li, Y. Yin, H. Yan, C. Lu, *Chem. Asian J*. **2017**, *12*, 2207–2210.
13. X. Li, H. Yan, Q. Zhao, *Chem. –Eur. J*. **2016**, *22*, 1888−1898.

14. S. Mukherjee, P. Thilagar, *Chem. Commun*. **2016**, *52*, 1070−1093.

15. L. Böhling, A. Brockhinke, J. Kahlert, L. Weber, R. A. Harder, D. S. Yufit, J. A. K. Howard, J. A. H. MacBride, M. A. Fox, *Eur. J. Inorg. Chem*. **2016**, 403−412.

16. L. Weber, J. Kahlert, R. Brockhinke, L. Böhling, J. Halama, A. Brockhinke, H.-G. Stammler, B. Neumann, C. Nervi, R. A. Harder, M. A. Fox, *Dalton Trans*. **2013**, *42*, 10982−10996.

17. J. Kahlert, L. Böhling, A. Brockhinke, H.-G. Stammler, B. Neumann, L. M. Rendina, P. J. Low, L. Weber, M. A. Fox, *Dalton Trans*. **2015**, *44*, 9766−9781.

18. B. H. Choi, J. H. Lee, H. Hwang, K. M. Lee, M. H. Park, *Organometallics* **2016**, *35*, 1771−1777.

19. M. Eo, M. H. Park, T. Kim, Y. Do, M. H. Lee, *Polymer* **2013**, *54*, 6321−6328.

20. T. Kim, H. Kim, K. M. Lee, Y. S. Lee, M. H. Lee, *Inorg. Chem*. **2013**, *52*, 160−168.

21. J. J. Peterson, A. R. Davis, M. Were, E. B. Coughlin, K. R. Carter, *ACS Appl. Mater. Interfaces* **2011**, *3*, 1796−1799.

22. D. Tu, P. Leong, Z. Li, R. Hu, C. Shi, K. Y. Zhang, H. Yan, Q. Zhao, *Chem. Commun*. **2016**, *52*, 12494−12497.

23. W. Zhang, Y. Luo, Y. Xu, L. Tian, M. Li, R. He, W. Shen, *Dalton Trans*. **2015**, *44*, 18130−18137.

24. L. Zhu, X. Tang, Q. Yu, W. Lv, H. Yan, Q. Zhao, W. Huang, *Chem. Eur. J*. **2015**, *21*, 4721−4730.

25. K.-R. Wee, Y.-J. Cho, S. Jeong, S. Kwon, J.-D. Lee, I.-H. Suh, S. O. Kang, *J. Am. Chem. Soc*. **2012**, *134*, 17982−17990.

26. Y. Chujo, K. Tanaka, *Bull. Chem. Soc. Jpn.* **2015**, *88*, 633−643.

27. M. Gon, K. Tanaka, Y. Chujo, *Polym. J*. **2018**, *50*, 109−126.

28. M. Gon, K. Tanaka, Y. Chujo, *Bull. Chem. Soc. Jpn*. **2019**, *92*. 7−18.

29. K. Nishino, K. Hashimoto, K. Tanaka, Y. Morisaki, Y. Chujo, *Tetrahedron Lett*. **2016**, *57*, 2025−2028.

30. K. Nishino, K. Uemura, K. Tanaka, Y. Chujo, *New J. Chem*. **2018**, *16*, 4210−4214.

31. K. Nishino, Y. Morisaki, K. Tanaka, Y. Chujo, *New J. Chem*. **2017**, *15*, 10550−10554.

32. H. Naito, K. Uemura, Y. Morisaki, K. Tanaka, Y. Chujo, *Eur. J. Org. Chem*. **2018**, 1885−1890.

33. K. Nishino, K. Uemura, K. Tanaka, Y. Chujo, *Molecules* **2017**, *22*, 2009−2018.

34. K. Tanaka, K. Nishino, S. Ito, H. Yamane, K. Suenaga, K. Hashimoto, Y. Chujo, *Faraday Discuss.* **2017**, *196*, 31−42.

35. H. Naito, K. Nishino, Y. Morisaki, K. Tanaka, Y. Chujo, *J. Mater. Chem. C* **2017**, *4*, 10047−10054.

36. K. Nishino, H. Yamamoto, K. Tanaka, Y. Chujo, *Org. Lett*. **2016**, *18*, 4064−4067.

37. H. Naito, K. Nishino, Y. Morisaki, K. Tanaka, Y. Chujo, *Chem. Asian J*. **2017**, *12*, 2134−2138.

38. K. Nishino, K. Uemura, K. Tanaka, Y. Morisaki, Y. Chujo, *Eur. J. Org. Chem*. **2018**, 1507−1512.

39. K. Nishino, K. Tanaka, Y. Morisaki, Y. Chujo, *Chem. Asian J*. DOI: 10.1002/asia.201801529.

40. K. Nishino, K. Hashimoto, K. Tanaka, Y. Morisaki, Y. Chujo, *Sci. China Chem*. **2018**, *61*, 940−946.

41. H. Mori, K. Nishino, K. Wada, Y. Morisaki, K. Tanaka, Y. Chujo, *Mater. Chem. Front*. **2018**, *2*, 573–579.

42. X. Li, H. Yan, Q. Zhao, *Chem. –Eur. J*. **2016**, *22*, 1888−1898.

43. S. Mukherjee, P. Thilagar, *Chem. Commun*. **2016**, *52*, 1070−1093.

44. K. Nishino, H. Yamamoto, K. Tanaka, Y. Chujo, *Asian J. Org. Chem*. **2017**, *6*, 1818−1822.

45. M. Kishimoto, K. Kondo, M. Akita, M. Yoshizawa, *Chem. Commun*. **2017**, *53*, 1425–1428.

46. J. Guo, D. Liu, J. Zhang, J. Zhang, Q. Miao, Z. Xie, *Chem. Commun*. **2015**, *51*, 12004– 12007.

47. S. J. Ladner, R. S. Becker, *J. Phys. Chem*. **1963**, *67*, 2481–2486.

48. H. Naito, K. Nishino, Y. Morisaki, K. Tanaka, Y. Chujo, *Angew. Chem., Int. Ed.* **2017**, *56*, 254–259.

49. B. P. Clarke, J. M. Thomas, J. O. Williams, *Chem. Phys. Lett.* **1975**, *35*, 251−254.

50. H. Liu, L. Yao, B. Li, X. Chen, Y. Gao, S. Zhang, W. Li, P. Lu, B. Yang, Y. Ma, *Chem. Commun.* **2016**, *52*, 7356−7359.

51. T. Higashi, ABSCOR. Program for Absorption Correction.; Rigaku Corporation: Japan, 1995.

52. G. M. Sheldrick, SHELX-97. Programs for Crystal Structure Analysis.; University of Göttingen: Germany, 1997.

53. K. Wakita, Yadokari&XG. Program for Crystal Structure Analysis; 2000.

54. L. J. Farrugia, *J. Appl. Cryst.* **1997**, *30*, 565−566.

## FIGURES AND TABLES

**Scheme 1.** Synthetic route of **CBAc**[a]

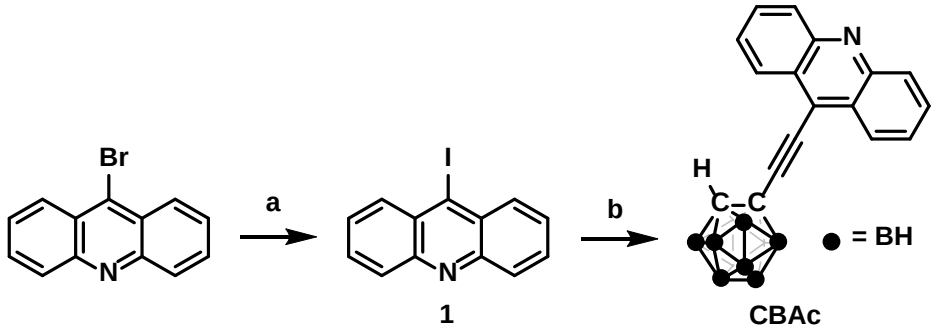


[a]Reagents and condition: (a) i) n-BuLi, diethylether, r.t., 30 min; ii) $I_2$, r.t., 16 h, 53% in two steps; (b) ethynyl-*o*-carborane, $Pd_2(dba)_3$, CuI, tri-2-furylphosphine, triethylamine, THF, r.t., 14 h, 24%.

**Table 1.** Photophysical properties of the acridine derivatives

| | $\lambda_{abs}$ (nm)[a] | $\varepsilon$ ($M^{-1}cm^{-1}$) | $\lambda_{em,solution}$ (nm)[a,b] | $\Phi_{PL}$[c] | $\tau$ (ns)[d] | $\lambda_{em,crystal}$ (nm)[b,e] | $\Phi_{PL}$[c] | $\tau$ (ns)[d] | $\lambda_{em,77K}$ (nm)[b,f] |
|---|---|---|---|---|---|---|---|---|---|
| **CBAc** | 372, 391, 413 | 17100 | 424, 448 | 0.06 | 0.25 (11%)<br>0.89 (89%) | 574 | 0.23 | 68 | 419, 446 |
| **TMSAc** | 370, 389, 411 | 14600 | 423, 446 | 0.13 | 1.41 | 480 | 0.11 | 13 (52%)<br>22 (48%) | 415, 441 |

[a] $1.0 \times 10^{-5}$ M in $CHCl_3$.

[b] Excited at 370 nm.

[c] Determined as an absolute value with the integration sphere method.

[d] Excited at 375 nm.

[e] Measured with the crystalline sample.

[f] $1.0 \times 10^{-5}$ M in 2-MeTHF.

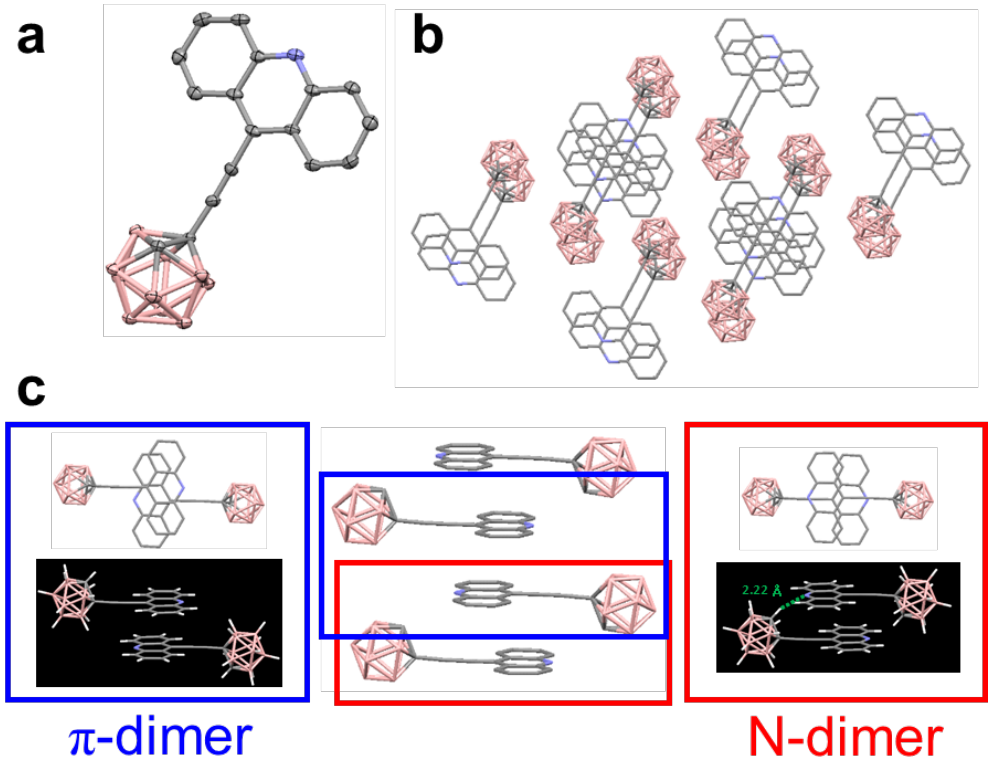


**Figure 1.** (a) Molecular structure of **CBAc** in crystal and (b) top and (c) side views of the crystal packing.

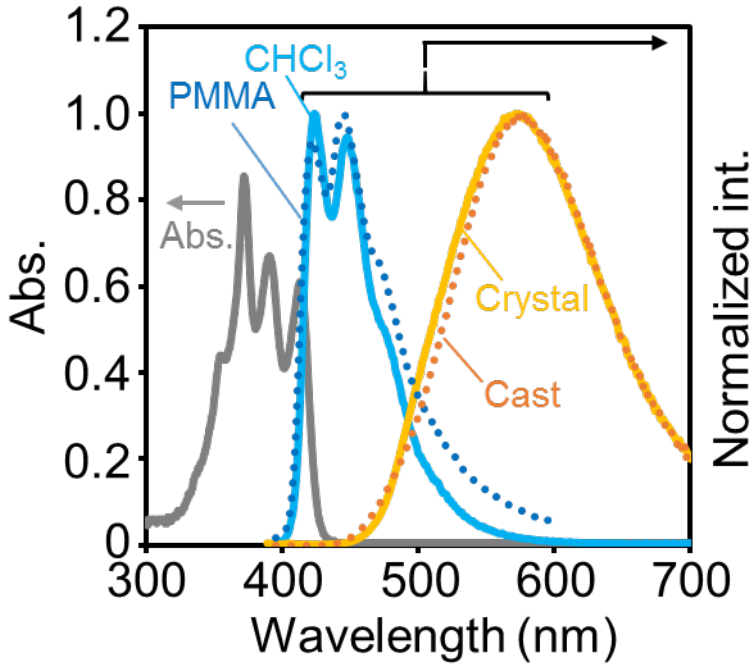


**Figure 2.** UV−vis absorption and PL spectra of the $CHCl_3$ solution and the solid samples of **CBAc**.

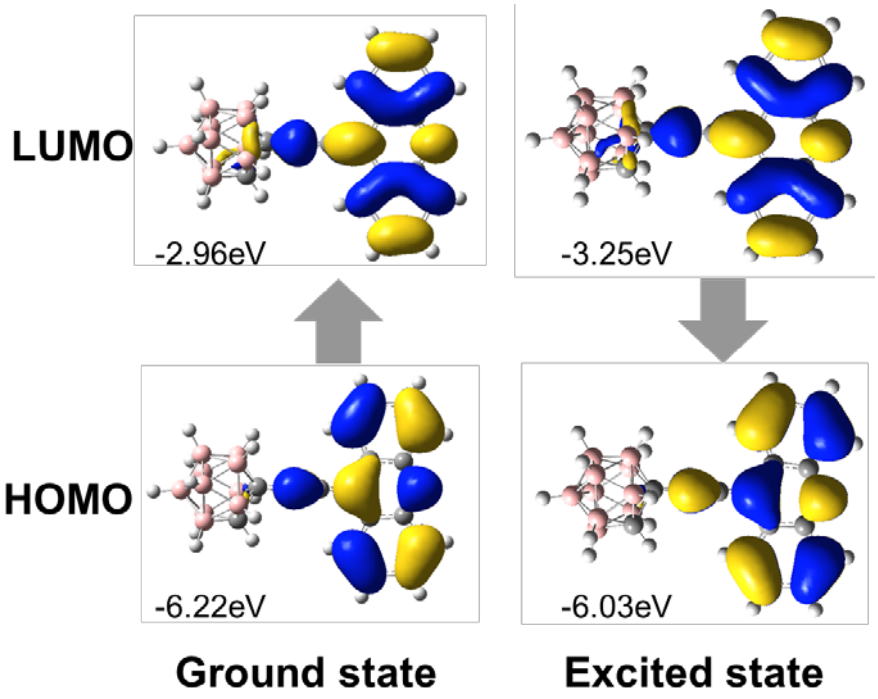


**Figure 3.** Molecular orbital distributions of **CBAc** in the ground and excited states calculated with DFT and TD-DFT calculations, respectively.

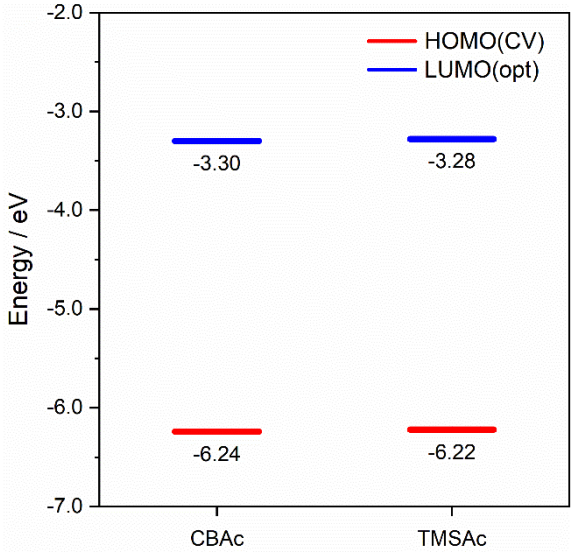


**Figure 4.** Energy levels of LUMO and HOMO of the acridine derivatives determined from optical and electrochemical data, respectively.

**GRAPHICAL ABSTRACT**

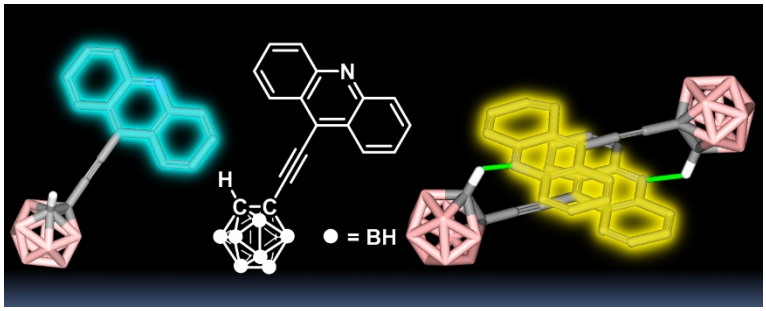


We report solid-state excimer emission based on the acridine−*o*-carborane dyad possessing the ethynyl spacer. Compared to the previous pyrene-modified *o*-carborane which showed excimer emission at 77 K in the crystalline state, the current acridine-modified molecule presented excimer emission with high efficiency at room temperature. It was indicated that two acridine moieties were stacked and the third acridine molecule was out of alignment. Furthermore, molecular interactions through the nitrogen atom in the acridine moiety and the hydrogen atom in the *o*-carborane unit contributes to improving emission efficiency in the crystalline state.

**Supporting Information index**


| | |
|---|---|
| -NMR data | Charts S1−S6 |
| -The structural data from X-ray analysis | Table S1 |
| -Other optical data | Figures S1−S5 |
| -Electrochemical data | Figure S6 |
| -The structural data obtained by quantum calculation | Table S2 |

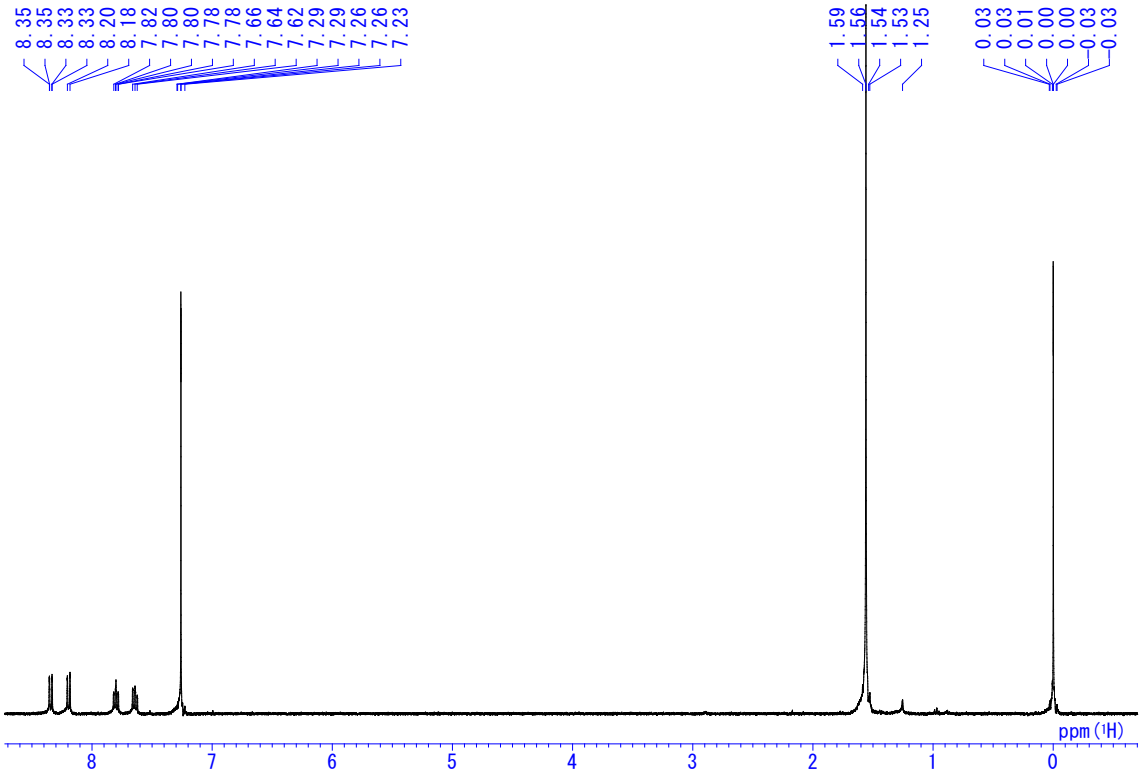


**Chart S1.** $^{1}$H NMR spectrum of 9-iodoacridine in $CDCl_3$.

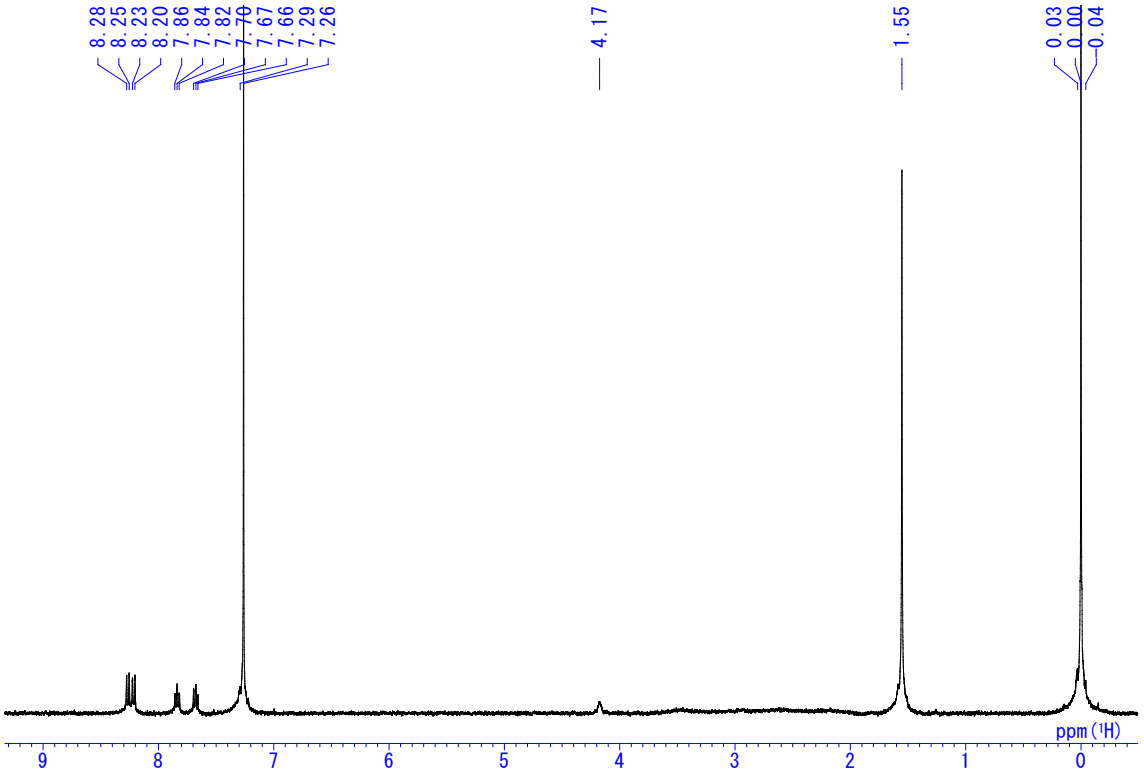


**Chart S2.** $^{1}$H NMR spectrum of **CBAc** in $CDCl_3$.

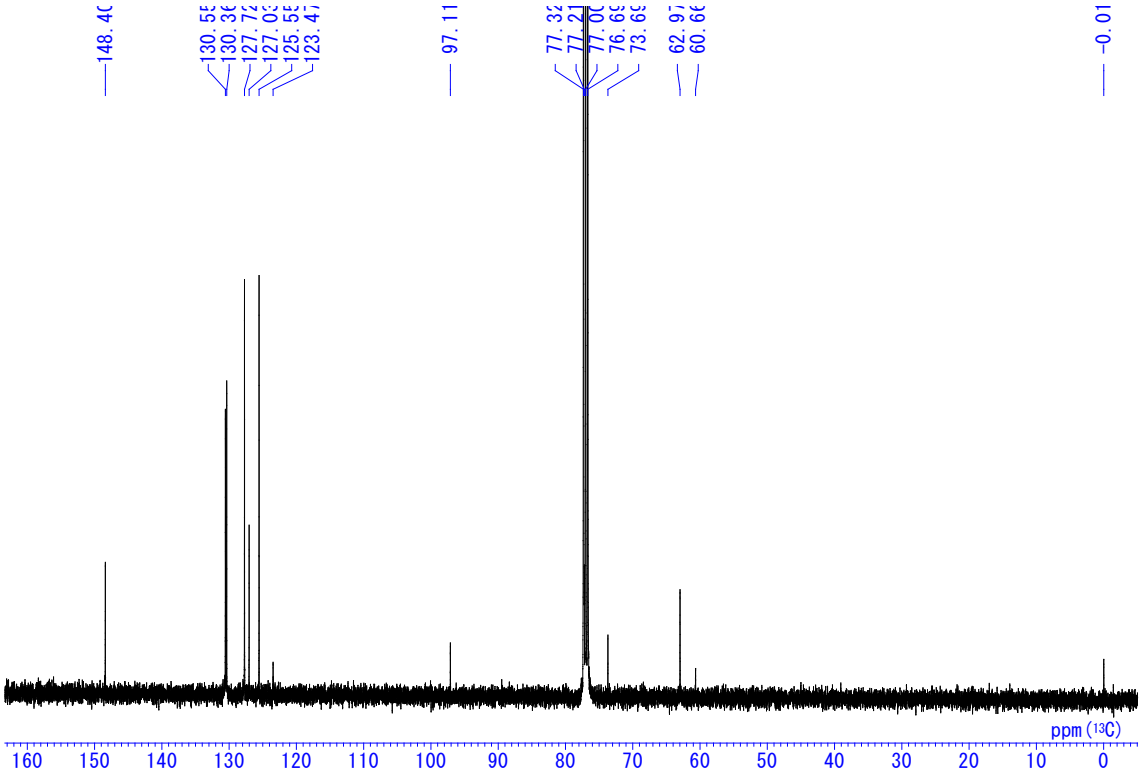


**Chart S3.** $^{13}C$ NMR spectrum of **CBAc** in $CDCl_3$.

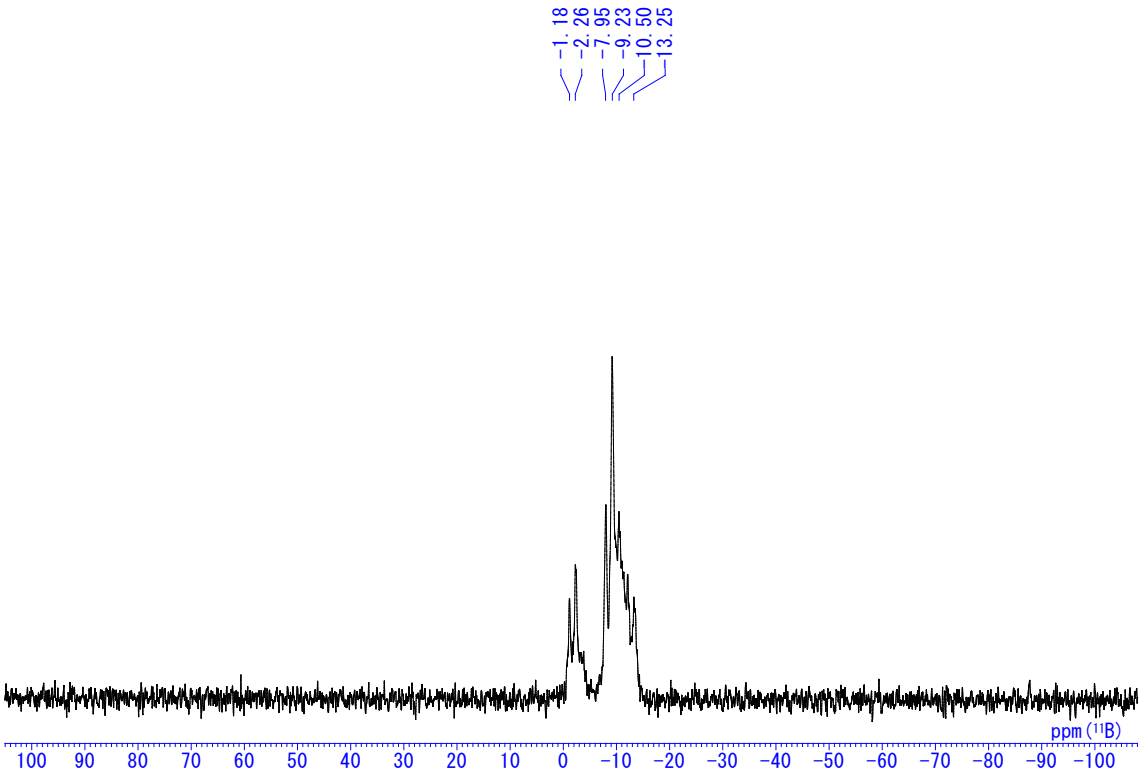


**Chart S4.** $^{11}B$ NMR spectrum of **CBac** in $CDCl_3$.

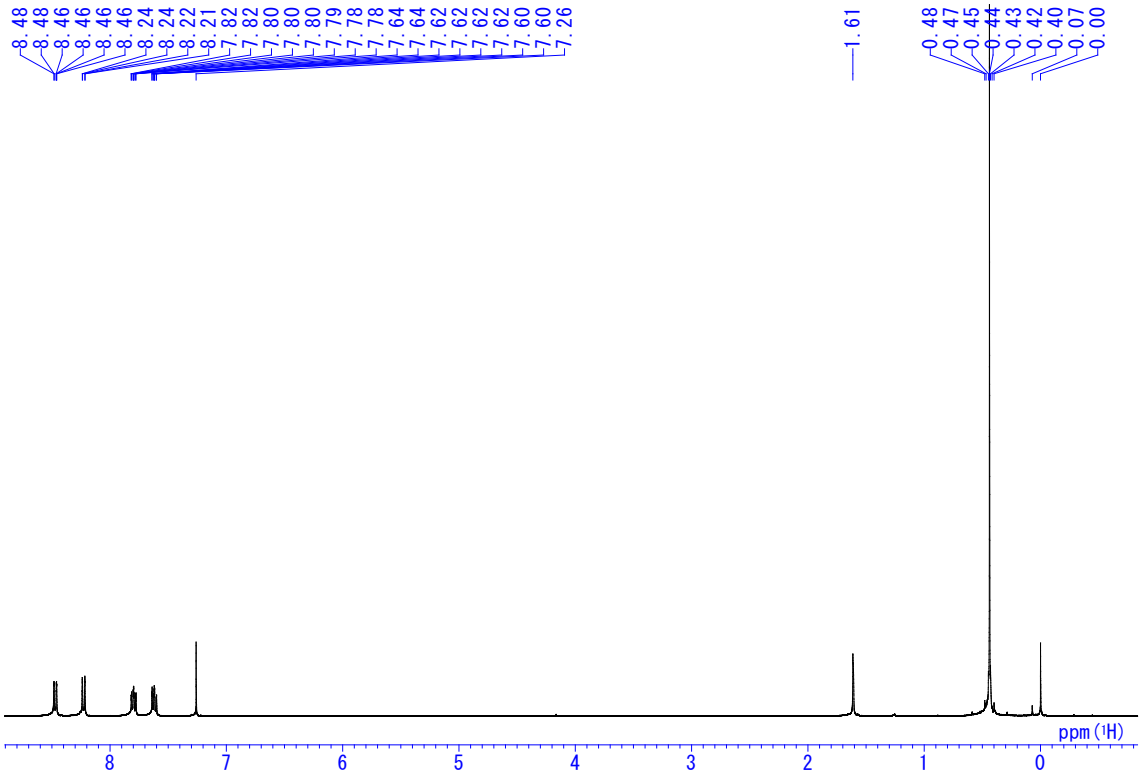


**Chart S5.** $^{1}$H NMR spectrum of **TMSAc** in $CDCl_3$.

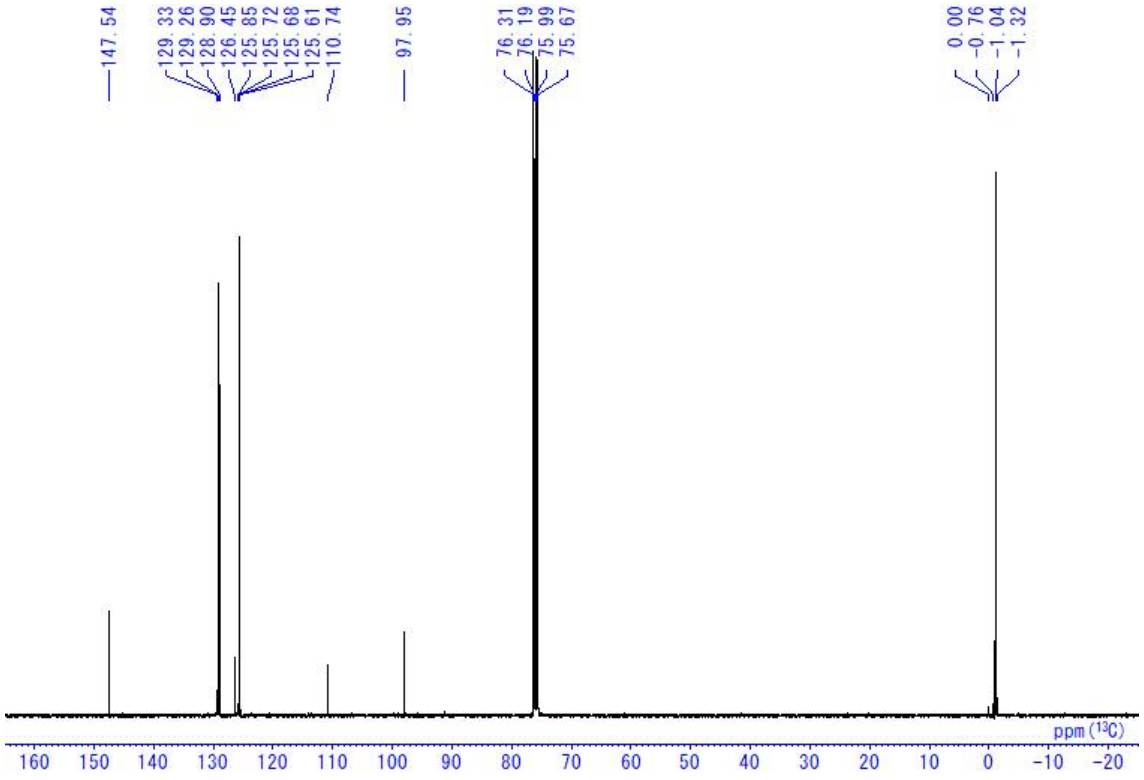


**Chart S6.** $^{13}$C NMR spectrum of **TMSAc** in $CDCl_3$.

**Table S1.** Crystallographic data of **CBAc**[a]

| | |
|---|---|
| Empirical formula | $C_{17}H_{19}B_{10}N$ |
| Formula weight | 345.43 |
| Temperature (K) | 97(2) |
| Wavelength (Å) | 0.71075 |
| Crystal system, space group | Triclinic, $P\ \bar{1}$ |
| Unit cell dimensions | $a$ = 6.9911(5) |
| | $b$ = 12.5718(10) |
| | $c$ = 12.7703(9) |
| | $\alpha$ = 60.809(4) |
| | $\beta$ = 78.088(5) |
| | $\gamma$ = 87.677(6) |
| $V$ (Å$^3$) | 956.37(13) |
| $Z$, calculated density (Mg m$^{-3}$) | 2, 1.200 |
| Absorption coefficient | 0.061 |
| $F$(000) | 356 |
| Crystal size (mm) | 0.50 × 0.30 × 0.10 |
| $\theta$ range for data collection | 2.99 –27.45 |
| Limiting indices | $-9\leq h\leq 8$, $-16\leq k\leq 16$, $-14\leq l\leq 16$ |
| Reflections collected (unique) | 9187/4324 [$R$(int) = 0.0630] |
| Goodness-of-fit on $F^2$ | 1.260 |
| Final $R$ indices [$I > 2\sigma(I)$][b] | $R_1$ = 0.0821, w$R_2$ = 0.1967 |
| $R$ indices (all data) | $R_1$ = 0.1331, w$R_2$ = 0.2352 |

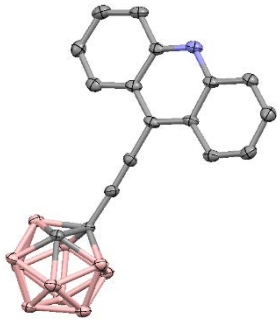

[a] The structures were solved by direct method (SIR97)[9] and refined by full-matrix least-squares procedures based on $F^2$ (SHELX-97).[10] [b] $R_1 = \Sigma(|F_0|-|F_c|)/\Sigma|F_0|$. w$R_2 = [\Sigma w(F^2_0-F^2_c)^2/\Sigma w(F^2_0)^2]^{1/2}$. $w = 1/[\sigma^2(F^2_0)+[(ap)^2+bp]]$, where $p = [\max(F^2_0,0)+2F^2_c]/3$.

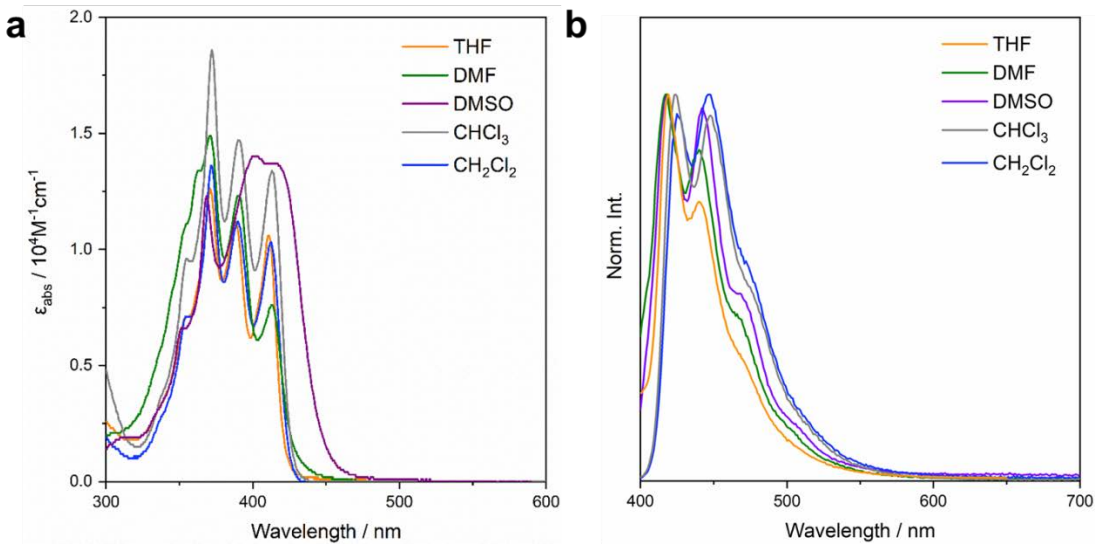


**Figure S1.** UV–vis absorption and PL spectra of **CBAc** in various solvents ($1.0 \times 10^{-5}$ M).

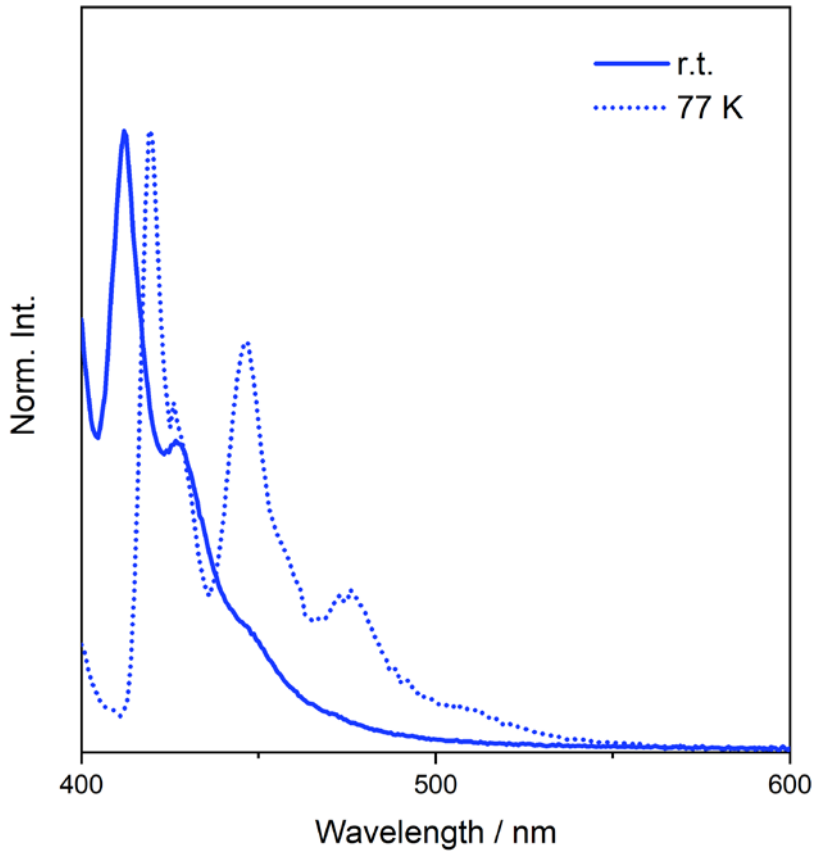


**Figure S2.** PL spectra of **CBAc** in 2-MeTHF at room temperature and 77 K ($1.0 \times 10^{-5}$ M).

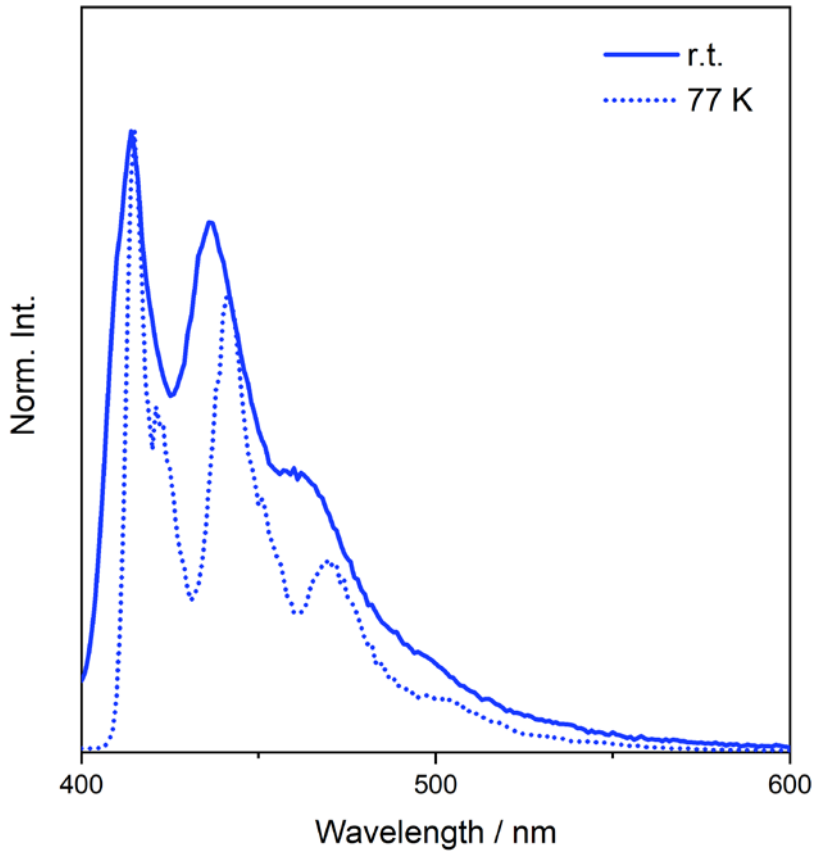


**Figure S3.** PL spectra of **TMSAc** in 2-MeTHF at room temperature and 77 K ($1.0 \times 10^{-5}$ M).

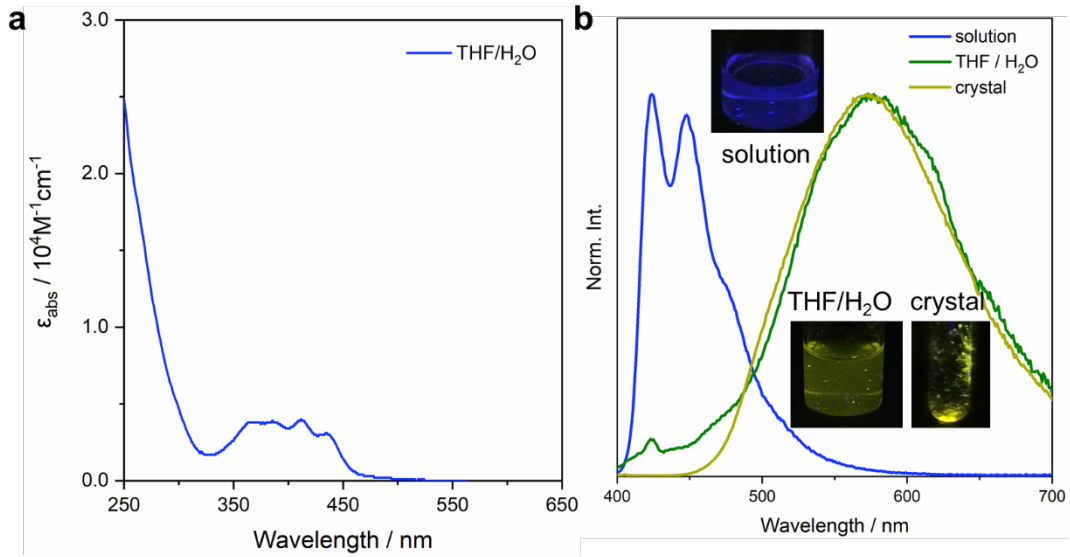


**Figure S4.** UV–vis absorption and PL spectra of **CBAc** in various solvent systems ($1.0 \times 10^{-5}$ M, in THF or THF/$H_2O$ = 1/99 v/v).

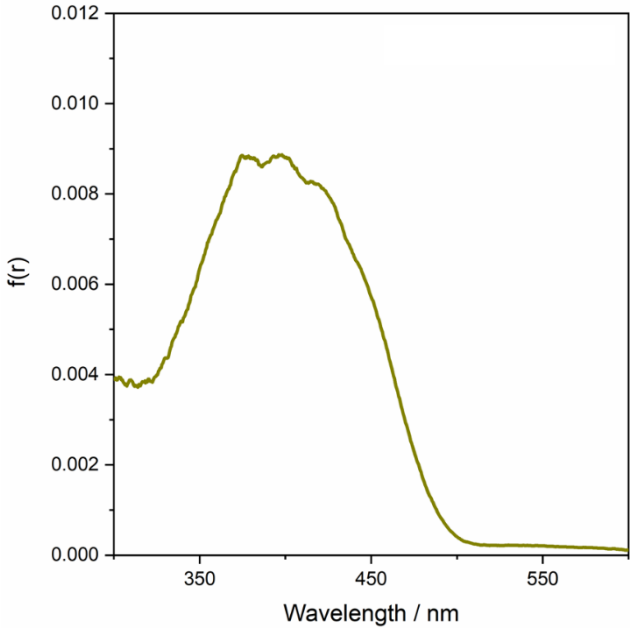


**Figure S5.** Diffusion reflection spectrum of the crystalline sample of **CBAc**.

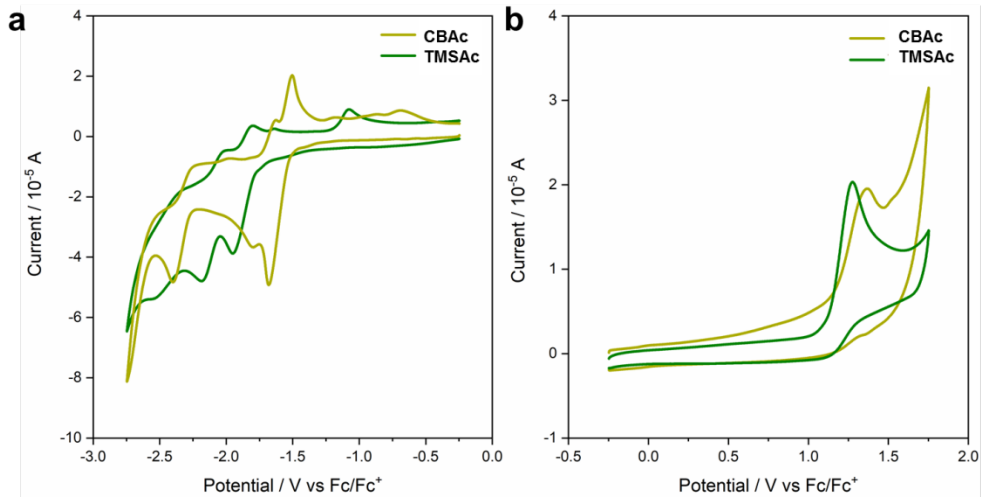


**Figure S6.** Cyclic voltammograms of **CBAc** and **TMSAc** in $CH_2Cl_2$ (1.0 mM) containing *n*-$Bu_4NPF_6$ (0.1 M) for (a) reduction and (b) oxidation.

**Table S2**. Cartesian coordinates of the optimized **CBAc** structure

| Center Number | Atomic Number | Atomic Type | Coordinates (Angstroms) X | Y | Z |
|---|---|---|---|---|---|
| 1 | 6 | 0 | 2.380100 | -1.222130 | 0.000765 |
| 2 | 6 | 0 | 3.822990 | -1.160800 | 0.000927 |
| 3 | 7 | 0 | 4.511070 | -0.007460 | 0.002730 |
| 4 | 6 | 0 | 1.669040 | 0.004000 | 0.000188 |
| 5 | 6 | 0 | 1.745770 | -2.500670 | -0.000063 |
| 6 | 6 | 0 | 2.493520 | -3.652080 | -0.001850 |
| 7 | 6 | 0 | 4.564270 | -2.385330 | -0.000831 |
| 8 | 6 | 0 | 3.948290 | 3.584850 | 0.002040 |
| 9 | 6 | 0 | 2.523930 | 3.654010 | -0.002390 |
| 10 | 6 | 0 | 1.767880 | 2.508010 | -0.003280 |
| 11 | 6 | 0 | -0.970050 | -0.017500 | -0.003790 |
| 12 | 6 | 0 | 3.832180 | 1.151150 | 0.002510 |
| 13 | 6 | 0 | 2.390120 | 1.223850 | -0.000082 |
| 14 | 1 | 0 | 1.996800 | -4.618590 | -0.002930 |
| 15 | 1 | 0 | 4.490070 | -4.519020 | -0.004340 |
| 16 | 6 | 0 | 3.918510 | -3.594650 | -0.002520 |
| 17 | 6 | 0 | 4.583290 | 2.369810 | 0.004200 |
| 18 | 1 | 0 | 4.527680 | 4.504290 | 0.002970 |
| 19 | 6 | 0 | 0.243840 | 0.003840 | -0.001100 |
| 20 | 1 | 0 | 0.661210 | -2.550230 | 0.000257 |
| 21 | 1 | 0 | 5.647470 | -2.310780 | -0.001140 |
| 22 | 1 | 0 | 5.665830 | 2.286120 | 0.006690 |
| 23 | 1 | 0 | 2.035570 | 4.624870 | -0.005840 |
| 24 | 6 | 0 | -2.402660 | -0.076520 | -0.014360 |
| 25 | 1 | 0 | 0.683570 | 2.565180 | -0.008650 |
| 26 | 6 | 0 | -3.245250 | 1.321920 | 0.248510 |
| 27 | 5 | 0 | -3.212550 | 0.151290 | 1.513530 |
| 28 | 5 | 0 | -3.211200 | 0.689030 | -1.355650 |
| 29 | 5 | 0 | -3.261650 | -1.078390 | -1.113660 |
| 30 | 5 | 0 | -3.261700 | -1.407380 | 0.646420 |
| 31 | 5 | 0 | -4.685630 | 1.057720 | 1.105170 |
| 32 | 5 | 0 | -4.683560 | 1.386870 | -0.646960 |
| 33 | 5 | 0 | -4.741930 | -0.705960 | 1.344760 |

| | | | | | |
|---|---|---|---|---|---|
| 34 | 5 | 0 | -4.740940 | -0.170520 | -1.511300 |
| 35 | 5 | 0 | -4.779820 | -1.467850 | -0.276170 |
| 36 | 5 | 0 | -5.664150 | 0.055120 | 0.009240 |
| 37 | 1 | 0 | -2.631910 | 2.199490 | 0.413900 |
| 38 | 1 | 0 | -2.523370 | 1.234510 | -2.146100 |
| 39 | 1 | 0 | -2.524770 | 0.372650 | 2.448010 |
| 40 | 1 | 0 | -2.617740 | -2.302340 | 1.077990 |
| 41 | 1 | 0 | -2.616440 | -1.755930 | -1.838890 |
| 42 | 1 | 0 | -5.034320 | 2.444040 | -1.051310 |
| 43 | 1 | 0 | -5.037040 | 1.896420 | 1.864870 |
| 44 | 1 | 0 | -5.253400 | -1.185150 | 2.302820 |
| 45 | 1 | 0 | -5.251690 | -0.268970 | -2.578270 |
| 46 | 1 | 0 | -5.324440 | -2.505020 | -0.470460 |
| 47 | 1 | 0 | -6.849520 | 0.120540 | 0.021010 |